nature physics

SUPPLEMENTARY INFORMATION

DOI: 10.1038/NPHYS1433

for the letter "Superconductivity in a single C_{60} transistor"

by C.B. Winkelmann *et al.*

1. Experimental Details

The data presented in this work were all acquired using the standard voltage or current biased lock-in technique. We have verified, namely for the Josephson current measurements, the numerically integrated $V_{ds}(I)$ curves not to be different from DC measurements. In particular no hysteresis was observed, even in DC current biased $V_{ds}(I)$ curves. Electromigration being up to date a difficult to control and statistical process, the use of two-wire measurements allowed to increase the experimental statistics. The experimental filtering is achieved by LC filters at room temperature followed by Π- and RC filtering at 40 mK through long coaxial lines (1.5 m per line, Thermocoax [1]), as already described in detail in [2]. A low impedance wiring setup has been shown to strongly favour the yield of well controlled nanogaps by electromigration [3]. Therefore a particular challenge to such experiments at dilution temperatures is the poor compatibility of the necessary electronic filtering with a low impedance environment. We minimize this constraint by relying on the high bandwidth feedback loop (1 MHz) for real-time monitoring of the junction conductance [2]. An independent test experiment on planar N-I-S junctions [4] showed that at cryostat base temperature our filtering setup reduces the effective electron temperature to below 80 mK.

As mentionned in the Methods section, we have used two types of superconducting electromigration junctions : (i) all aluminum junctions, and (ii) hybrid Au/Al junctions. In the later, a thin (10 nm) and continuous Au wire is first deposited, which is then covered by much thicker (typically 100 nm) Al electrodes. The second deposition is performed at smaller evaporation angles, so that the aluminum electrodes *do not overlap* (fig. S1a). The weakest link of the devices comes from the central overlap of gold and after the electromigration process the fullerene is therefore in contact with a gold surface, in which superconductivity is proximity induced by the much thicker aluminum reservoirs. The use of two different types of junction materials allowed to explore different strengths of the tunnel coupling and of the superconducting correlations. All aluminum junctions tend to display strongly developped superconducting properties after electromigration, characterized by a tunneling spectrum

DOI: 10.1038/NPHYS1433

markedly ressembling a BCS density of states in the low bias regime after electromigration. However, the QD devices that were obtained from all aluminum wires generally displayed a rather weak tunnel coupling to the leads, with charging energies usually dominating the other relevant energy scales (e.g. devices A and C). On the other hand, the tunnel junctions obtained by electromigration in Au/Al junctions, irrespective of their gate dependence, displayed more rounded superconducting tunneling features, as can be expected in superconducting proximity structures. We observed several molecular QD devices of this type to exhibit a stronger tunnel coupling to the leads, which may be due to a better electronic coupling of fullerenes to gold than to aluminum surfaces, associated to different surface reactivities [11] (e.g. devices B and D). While in Au/Al junctions superconductivity vanishes at fields of about 30 mT, H_c can reach a fraction of a Tesla in all aluminum junctions. In the later indeed, the relevant superconducting correlations originate from the statistically quite nanostructured edges of the aluminum tunnel junctions in the vicinity of the molecular QD, while in the hybrid junctions, superconductivity is induced in the gold leads by the much bulkier aluminum contacts, with a critical field therefore close to the bulk value in aluminum. In nanostructured aluminum, it is established that superconductivity can stabilize up to fields exceeding 1 Tesla [15].

2. Device A

In a SMT, the junction capacitance C_j is defined as $C_j = C_s + C_d + C_g$, with parameters as defined in figure S 1b. Device A (figure 1b) has a very large addition energy $E_{add} \geq 250\,\mathrm{meV}$. Identifying E_{add} and the charging energy $E_c = e^2/C_j$ gives an upper bound of 0.32 aF to the junction capacitance. From the slopes of the CD edges, we determine the relative weights of its components to be such that $C_d = 1.49 \times C_s = 12.7 \times C_g$. We use this order of magnitude of C_j namely as an input for estimating the Josephson junction quality factor in device D. The asymmetry of the current steps across the CD edges of opposite bias voltage sign allows to determine a coupling asymmetry $\Gamma_d/\Gamma_s \approx 4$ (Ref. [5]). From the $I(V_{ds})$ characteristics at high bias, we further extract $\Gamma = (\Gamma_s\Gamma_d)/(\Gamma_s + \Gamma_d) \approx 1\,\mu\mathrm{eV}$, corresponding to the weak coupling limit.

It is notable that device A does not show any negative differential conductance (NDC) effect in the superconducting state. NDC is expected e.g. when a superconducting lead

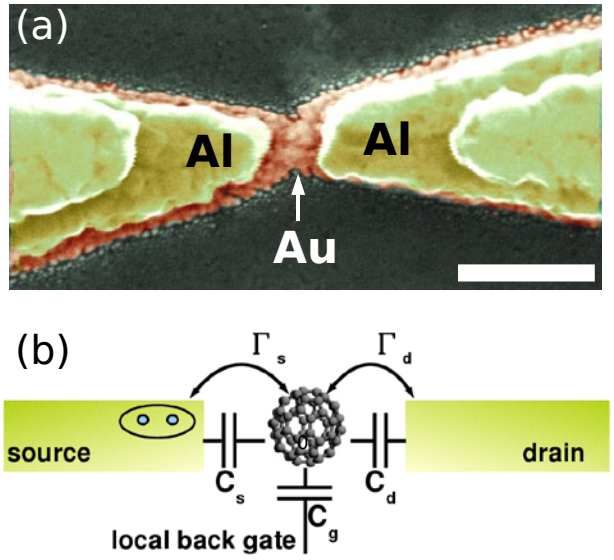

Fig. S 1: (a) Colored SEM image of a hybrid Au/Al wire prior to electromigration. The thin Au leads (red) slightly overlap, the thicker Al electrodes (yellow) are 80 nm apart. The scale bar is 200 nm. (b) Schematics of the capacitive and tunnel couplings of the SMT with superconducting leads.

DOS couples to a sharp dot state : at energies slightly above the conduction resonance, the contributing lead DOS, and therefore the current, decrease. This was previously observed in metallic nanoparticles [6], carbon nanotubes [7] and semi-conducting nanowires [8] coupled to superconducting leads. The effect is also seen in our device C. In device A however, the linewidths of the spectroscopic levels are about 100 μeV (accounting for a capacitive division coefficient close to 0.5), which largely smears the effect of the superconducting leads' coherence peaks. Temperature can account for a broadening of $3.5k_BT = 24\,\mu eV$ ($T_{elec} = 80$ mK), while finite lifetime effects associated to the lead coupling can be estimated from the current steps not to exceed a few μeV. Finally, the 40 μV lock-in voltage modulation will also induce a $\approx 20\,\mu eV$ energy smearing. Summing up all these contributions suffices to explain about half of the experimental broadening. However, while level linewidths of 10 μeV in 2DEGs and down to 25 μeV in metallic nanoparticles have been observed, it is notable that in single molecule transistors, even for weak lead coupling and electronic temperatures below 100 mK, the linewidths systematically exceed the 100 μeV range [9, 10].

DOI: 10.1038/NPHYS1433

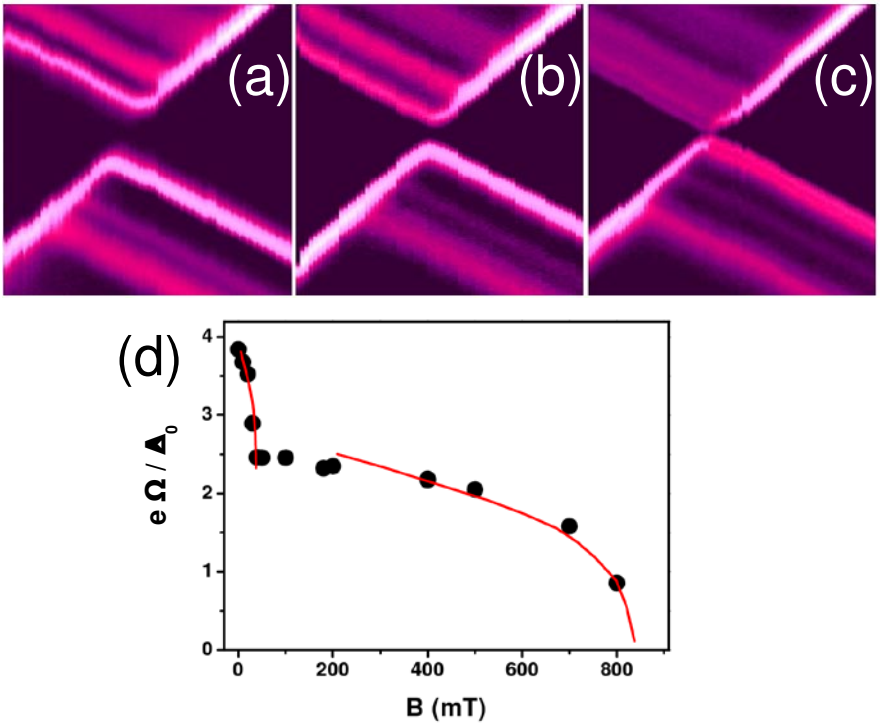

Fig. S 2: (a) to (c) Differential conductance map as a function of V_g (horizontal axis) and V_{ds} voltage (vertical axis) for magnetic fields respectively 0 T, 400 mT and 800 mT. The gate voltage window spanned is 23 mV, the bias voltage window spanned is 3.2 mV. (d) The progressive suppression of the spectroscopic gap can be qualitatively described by introducing a pair breaking energy $\propto B^2$ (see text). The lines are fits to the data from figure 1c, associated to the S to N transition of each electrode. The only adjustable parameter is the value of critical field.

The gradual vanishing of the spectroscopic gap Ω in device A under magnetic field is shown in figure S 2. In a nanoscopic junction, of dimensions smaller than the London penetration length, the $\Omega(B)$ dependence can be described assuming a pair breaking energy $\gamma \propto B^2$ [12]. The comparison of the data to the magnetic field dependence of the half-excitation energy gap as calculated by Skalski *et al.* [12] is shown in figure S 2d. Such a model can however only very qualititatively apply to the particular geometry of electromigrated single molecular junctions (figure S 2d).

3. Device B

Moving on to device B, the right CD in figure 2c (main paper) shows a Kondo resonance

and thus corresponds to an odd electron occupation number. In the left CD ($V_g < -1.7\,\mathrm{V}$, even occupation number), a gate-independent transition at a finite bias of 4 mV is observed. Such features are generally attributed to inelastic cotunneling channels. Further, in all devices the background conductance in the Coulomb blockade regions is not stricly nil, and can span values between 1 % and 90 % of the maximum overall conductance. We attribute this to a parallel direct tunneling channel from source to drain, partly shunting the QD and therefore insensitive to the gate potential. In this particular device, the large addition energy is again clearly pointing to a molecular QD, all the more as the strong environmental coupling significantly contributes to decreasing the dot charging energy [13, 14]. The superconducting features disappear for magnetic fields above 30 mT, the Kondo energy scale however is too large for the Kondo resonance to be split by our experimentally accessible fields.

4. Device C

On scanning the gate voltage, device C was subject to telegraphic noise (figure S 3a). This bistability of the conductance, probably of either electrostatic or mechanical nature [16], hindered very detailed measurements. Its Coulomb blockade and Kondo resonance pattern in the normal state is shown in figure S3a. A Kondo temperature $\mathrm{T}_K = 0.7\,\mathrm{K}$ is extracted from a mean resonance peak FWHM=$120\,\mu$V. The onset of superconductivity (figure S 3b) produces the negative differential conductance behavior already discussed for figure 2b. It is seen here that the effect is strongest close to the degeneracy points. A closer look at the magnetic field dependence of the low bias conductance in figure 2d reveals that the negative differential conductance effect disappears around 20 mT, long before the superconducting coherence peaks merge into the Kondo resonance.

5. Device D

Similarly to break-junctions [20], nanogaps provide a locally resistive environment which strongly affects the transport properties in terms of a Josephson weak link [19]. The effect of the electromagnetic environment on small Josephson junctions is usually described by the "particle in a washboard potential" picture [17]. We assume for device D environmental RC parameters as described in figure S 4. If current biased through an environment of resistance R, the quality factor of the junction writes [18]

DOI: 10.1038/NPHYS1433

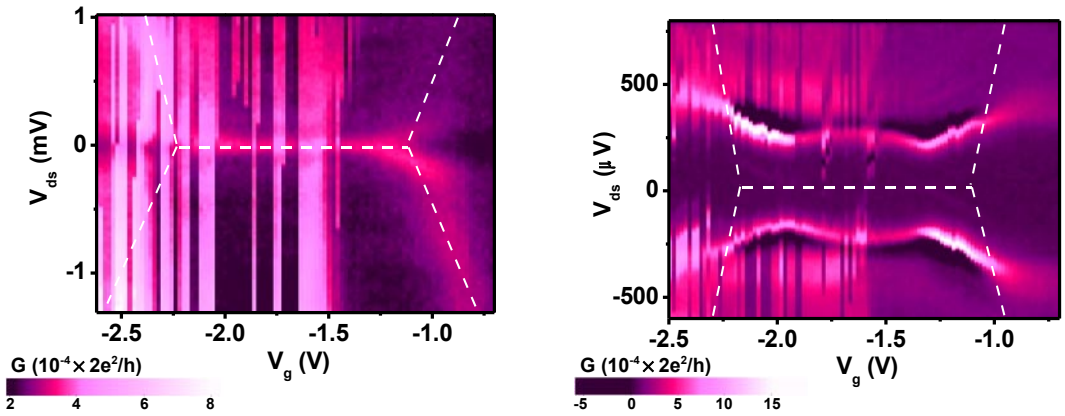

Fig. S 3: (a) Differential conductance map of device C as a function of gate and bias voltage in the normal state (T = 40 mK, B = 400 mT). The dotted lines emphasize the CD edges. (b) Same measurement in the superconducting state (B = 0 T). Large regions of negative differential conductance appear at bias voltages slightly above the quasiparticle coherence peaks.

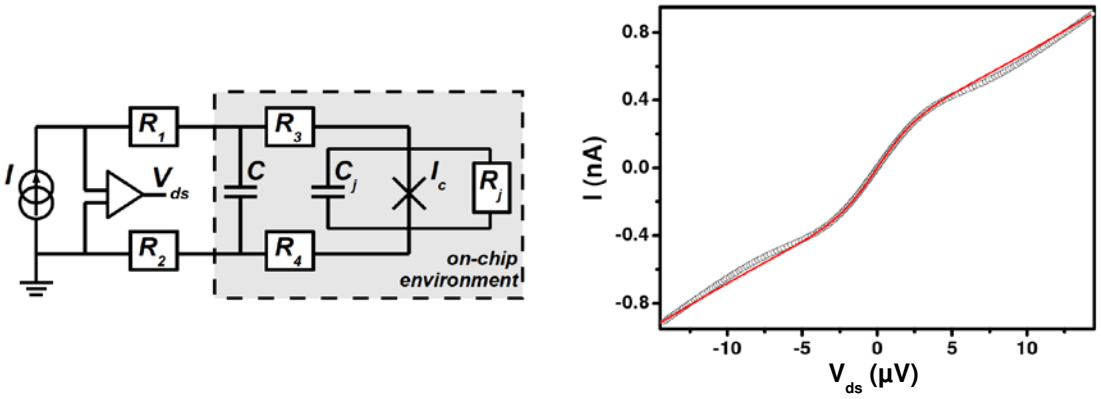

Fig. S 4: (a) Schematics of the current biased setup. The Josephson junction of critical current I_c is in parallel with the junction capacitance C_j and the junction normal state resistance R_j, which is tuned by V_g. The junction environment is further given by a series resistance $R = R_1+R_2+R_3+R_4$, both on and off chip, and a parallel capacitance C which is dominantly on-chip. (b) $I(V_{ds})$ at $V_g = 3\,\mathrm{V}$ (bullets) and best fit to eq. 2 (line) assuming $R = 1350$ Ohm and an effective electron temperature $T = 70$ mK. The fit yields $I_c = 1.39$ nA.

$$Q = \frac{1}{RC + \hbar/(2eI_cR_j)}\sqrt{\hbar/(2eI_cR_j)((R_j+R)C + R_jC_j)}. \qquad (1)$$

The junction capacitance C_j is very small, below 1 aF as determined from the weak coupling

data. From capacitance measurements of the device to the local backgate before electromigration, we estimate $C \approx 2\,\mathrm{pF}$. Taking further $I_c \approx 1\,\mathrm{nA}$, $R \approx 1\,\mathrm{k\Omega}$ and $R_j \approx R_K$ leads to a quality factor $Q \approx 1$. Device D is thus in the cross-over regime from the weak to the large friction limit. The transport characteristics of an overdamped ($Q \ll 1$) junction are given by :

$$I(V_{ds}) = \frac{R_j}{R_j + R}\left\{ I_c \,\mathrm{Im}\left(\frac{I_{1-i\eta}(E_J/k_BT)}{I_{-i\eta}(E_J/k_BT)} \right) + \frac{V_{ds}}{R_j} \right\}, \qquad (2)$$

where $\eta(V_{ds}) = \hbar V_{ds}/(2eRk_BT)$, $E_J = I_c\hbar/2e$ is the Josephson energy, and $I_\alpha(x)$ is the modified Bessel function of complex order α [17, 19]. As device D is not strictly in the overdamped limit, a fit using eq. (2) can approximately describe the data but fails to reproduce the experimentally more marked switching behavior for $I \approx I_s$ (figure S 4b). A complete analysis valid for arbitrary damping [21] is beyong the scope of this work.

[1] www.thermocoax.com

[2] Roch, N., Florens, S., Bouchiat, V., Wernsdorfer, W. & Balestro, F. Quantum phase transition in a single-molecule quantum dot. *Nature* **453**, 633 (2008).

[3] van der Zant, H.S.J. *et al.* Molecular three-terminal devices: fabrication and measurements. *Faraday Diss.* **131**, 347 (2006).

[4] Al/Cu junctions provided by S. Rajauria and H. Courtois.

[5] Bonet, E., Deshmukh, M.M. & Ralph, D.C. Solving rate equations for electron tunneling via discrete quantum states. *Phys. Rev.* **B 65**, 045317 (2002).

[6] Ralph, D.C., Black, C.T. & Tinkham M. Spectroscopic measurement of discrete electronic states in single metal particles. *Phys. Rev. Lett.* **74**, 3241-3244 (1995).

[7] Eichler, A., *et al.* Even-Odd Effect in Andreev Transport through a Carbon Nanotube Quantum Dot. *Phys. Rev. Lett.* **99**, 026601 (2007).

[8] Doh, Y.-J., De Franceschi, S., Bakkers, E.P.A.M. & Kouwenhoven, L.P. Andreev Reflection versus Coulomb Blockade in Hybrid Semiconductor Nanowire Devices. *Nano Lett.* **8**, 4098-4102 (2008).

[9] Park, J., *et al.* Coulomb blockade and the Kondo effect in single-atom transistors. *Nature* **417**, 722-725 (2002).

DOI: 10.1038/NPHYS1433

[10] Grose, J.E., *et al.* Tunneling Spectra of Individual Magnetic Endofullerene Molecules. *Nature Mater.* **7**, 884-889 (2008).

[11] Maxwell, A.J., Brühwiler, P.A., Arvanitis, D., Hasselström, J., Johansson, M.K.-J. & Martensson, N. Electronic and geometric structure of C60 on Al(111) and Al(110). *Phys. Rev.* **B 57**, 7312 (1998).

[12] Skalski, S., Betbeder-Matibet, O. & Weiss, P.R. Properties of Superconducting Alloys Containing Paramagnetic Impurities. *Phys. Rev.* **136**, A1500 (1964).

[13] Kaasbjerg, K. & Flensberg, K. Strong Polarization-Induced Reduction of Addition Energies in Single-Molecule Nanojunctions. *Nano Lett.* **8**, 3809 (2008).

[14] Thygesen, K. & Rubio A. Renormalization of Molecular Quasiparticle Levels at Metal-Molecule Interfaces: Trends across Binding Regimes. *Phys. Rev. Lett.* **102**, 046802 (2009).

[15] Black, C.T., Ralph, D.C. & Tinkham M. Spectroscopy of the Superconducting Gap in Individual Nanometer-Scale Aluminum Particles. *Phys. Rev. Lett.* **76**, 688 (1996).

[16] Danilov, A.V., Hedegard, P., Golubev, D.S., Bjornholm, T. & Kubatkin, S.E. Nanoelectromechanical Switch Operating by Tunneling of an Entire C60 Molecule. *Nano Lett.* **8**, 2393 (2008).

[17] Ivanchenko, Yu.M. & Zilberman, L.A. The Josephson Effect on Small Size Tunnel Contacts. *Sov. Phys. JETP Lett.* **28**, 1272 (1969).

[18] Jarillo-Herrero, P., van Dam, J.A. & Kouwenhoven, L.P. Quantum supercurrent transistors in carbon nanotubes. *Nature* **439**, 953 (2006).

[19] Jørgensen, H.I., Novotný, T., Grove-Rasmussen, K., Flensberg, K. & Lindelof, P.E. Critical Current 0-π Transition in Designed Josephson Quantum Dot Junctions. *Nano Lett.* **7**, 2441 (2007).

[20] Chauvin, M., vom Stein, P., Esteve, D., Urbina, C., Cuevas, J.C. & Levy Yeyati, A. Crossover from Josephson to Multiple Andreev Reflection Currents in Atomic Contacts. *Phys. Rev. Lett.* **99**, 067008 (2007).

[21] Ambegaokar, V. & Halperin, B.I. Voltage Due to Thermal Noise in the dc Josephson Effect. *Phys. Rev. Lett.* **22**, 1364 (1969).